An N-port system model for multiwinding transformer based multilevel converters in DC-autotransformer configuration

Ferdinand Grimm, Mehdi Baghdadi and Richard Bucknall
Faculty of Engineering Sciences
University College London
London WC1E 6BT, United Kingdom
Email: ferdinand.grimm.18@ucl.ac.uk

***Abstract*—This paper proposes a time-domain modelling approach for a multi-winding transformer-based multilevel DC/DC converter. Within previous research, multi-winding transformers have been modeled using cantilever models. These models, while simple, have no direct intuitive interpretation. Furthermore, they do not include currents circulating within each individual module and external load currents affecting only some of the modules at the same time. In this paper, a DC/DC converter model that includes the transformer as N- port network with magnetization and stray inductance and conduction losses is proposed. The model is verified using simulations showing both accurate predictions of both, circulating currents within each module and load currents affecting multiple modules.**

I. Introduction

The multi-active bridge [1] is a multi-winding isolated DC/DC converter topology and forms a multiport extension of the well-known dual-active bridge topology [2].
Converters based on multi-active bridges can be found in numerous applications including computing centers [3], energy routers [4], and battery balancers [5].
A promising approach for a DC/AC converter based on multi-active bridges has been proposed in [6]. The authors use a multi-active bridge to create different voltage levels and apply a tap selector to convert the voltage to AC. To ensure an increase in DC voltage, the multi-active bridge modules are furthermore connected in series.
The lumped circuit modeling of multi winding topologies has been studied for several decades with the two most prominent ones being based on leakage transformers [7] or the cantilever model [8]. Either of these models can be reformulated into the N-port model which does not explicitly include cross-coupling effects. Both these modeling approaches rely on a set of parameters that have to be determined either by experimental measurements [9], finite elements [10], or in some cases by analytic computations [11], [12]. To analyze the behavior of multi-active bridges, a continuous system model has been developed in [13] for the case of a transformer with stray inductances and in [14] a model for a multi winding transformer has been provided in a mesh configuration. While the modeling of the transformer is detailed it does not include modeling of the rectifier part and requires a matrix inversion. In [15], a detailed continuous model has been developed for the special case of a triple active bridge and an average model was subsequently derived. The authors of [16] and [17] further analyzed the power distribution in multi-active bridges and provided controller solutions based on the average model. Another modeling approach has been proposed in [18]. The authors develop a model for a multi-winding transformer-based solid-state transformer. Based on the assumption of equal winding currents and equal modules, a system differential equation is formulated and examined.
In this paper, we propose a novel system model in the time domain for this circuit which includes the dynamics of the DC-link of each module. Including the DC-link dynamics of each module allows us to use the model to investigate module balancing effects and the currents that will be flowing through the system during the balancing. The system model is derived in star connection and requires no matrix inversion or knowledge of virtual branch inductances. For the proposed model, only quantities concerning a certain module will be chosen as state-space variables. The model can therefore be used to examine the detailed transient phenomena occuring within each module such as current transients as well as phenomena occuring in the whole circuit such as charge balancing.

II. System Topology

An overview of the system topology is given in Fig. 1. The system considered in this paper consists of a DC-side and an AC-side. The DC-side and AC-side are linked through M DC/AC modules. that allows for bidirectional power flow between modules. On the AC side, the modules are connected by a multi-winding transformer. Each of the windings in the multi-winding transformer shares the same core and thus the same flux Φ_M. In this paper, it is assumed that all windings have the same number of turns. The windings convert the flux to an AC voltage, achieving a magnetic equivalent of a parallel connection between modules. In case an active bridge such as the one shown in Fig. 3a is used as a topology for the submodules, the AC-side together with the active bridge modules form a multi-active bridge converter like the

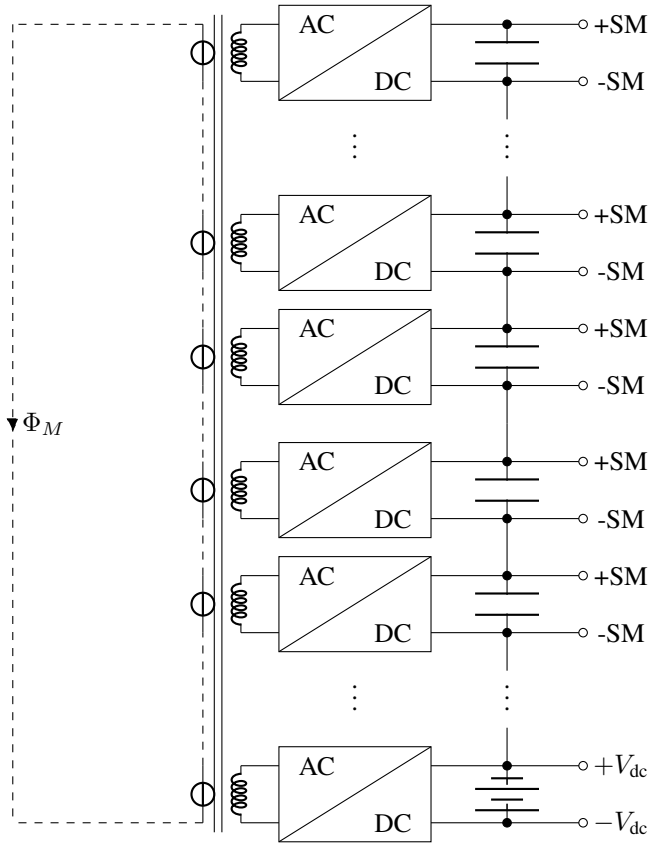

Figure 1: Basic working principle of the DC-autotransformer. AB represents an active bridge. The ports +SM and -SM can be connected to any submodule topology introduced earlier or a tap selector. Electric connections are drawn solid and magnetic connections are drawn dashed.

one described in e.g. [1]. On the DC-side, the active bridge modules are connected in series [6]. In this way, during steady-state operation, the DC-output voltage of each active bridge can be expressed as an integer multiple of the individual bridge voltage. In the following, this topology will be referred to as DC-autotransformer, since the voltages at different modules of the DC-side of the converter concerning ground add up like the voltages of a tapped autotransformer. As a power supply, the lowest of the modules is connected to a voltage source with a fixed voltage V_{dc}. The connection of the load to the circuit diagram is shown in Fig. 2. A load can be connected between any port of the DC-autotransformer and the $-V_{\text{dc}}$ port allowing to achieve different output voltages. The circuit can be used as a multilevel inverter as well, by changing the DC-voltage level of the load.

III. Multiactive Bridge Model

The model is based on a multi-winding [19] formulation of the dual-active bridge model. For the modeling, the following assumptions will be used:

- All MOSFETs behave like ideal switches, switching instantaneously with no internal dynamics except for their ON-state resistance.
- All nonlinearities such as hysteresis properties of the materials and temperature dependencies are negligible.
- The transformer has a homogeneous flux that is constant over all modules. All cross-coupling between two modules is negligible.
- All interwinding and intra-winding capacitances are negligible.
- All modules are identical, i.e. have the same switches, windings, turn numbers, DC-link capacitors, and track wirings.
- Frequency dependencies of the parameters as well as high-frequency effects such as the proximity effects and the skin effect in the transformer are negligible.

In addition to that, it is assumed that MOSFETs are used as switches in the following. The derivation however can be generalized to other switch technologies such as IGBTs or MCTs assuming their behaviour can be modelled with a single Ohmic resistor during the ON-state. Using these assumptions, the active bridge topology can be modelled with the equivalent circuit shown in Fig. 3b. The resistors can furthermore be summarized into a simplified circuit with a (time-varying) source and internal resistance as seen in Fig. 3c. Assuming that all modules are identical i.e. the conduction resistance R, DC-link capacitance C_{dc}, number of turns N, and stray inductance L_s have the same value for each module. The value of R is depending on the cell topology, for dual active bridge cells it is given as $R = R_s + 2R_{ON}$, where R_s is the winding resistance and R_{ON} is the ON-state resistance of the switch. The model is set up from the point of view of the transformer. Each module has a certain switching state $s_k(t) \in \{-1, 1\}$ which determines the relationship between the DC-voltage $V_k(t)$ and AC-current $i_k(t)$. The current differential equation for an arbitrary module is given as:

$$\frac{\mathrm{d}}{\mathrm{d}t} i_k = \frac{V_{L_k}}{L_s}. \tag{1}$$

Using Kirchhoffs voltage law we can reformulate V_{L_k} as:

$$\frac{V_{L_k}}{L_s} = \frac{1}{L_s} V_k \cdot s_k(t) - \frac{R}{L_s} i_k - \frac{R_m}{L_s} i_m - \frac{L_m}{L_s} \frac{\mathrm{d}i_m}{\mathrm{d}t}. \tag{2}$$

An M-module DC-autotransformer has $2M + 1$ reactive elements, M DC-link capacitors, M winding inductors, and the magnetization inductance. However, only $2M$ of them have linearly independent states as the magnetization current can be expressed as a linear combination of the others:

$$\begin{aligned} \frac{\mathrm{d}i_m}{\mathrm{d}t} &= \frac{\mathrm{d}}{\mathrm{d}t} \left(\sum_{i=1}^{M} i_i \right) && (3) \\ &= \sum_{i=1}^{M} \frac{1}{L_s} V_i \cdot s_i(t) - \sum_{i=1}^{M} \frac{R}{L_s} i_i + \\ &\quad - \sum_{i=1}^{M} \frac{R_m}{L_s} \cdot i_m - \sum_{i=1}^{M} \frac{L_m}{L_s} \frac{\mathrm{d}i_m}{\mathrm{d}t}. && (4) \end{aligned}$$

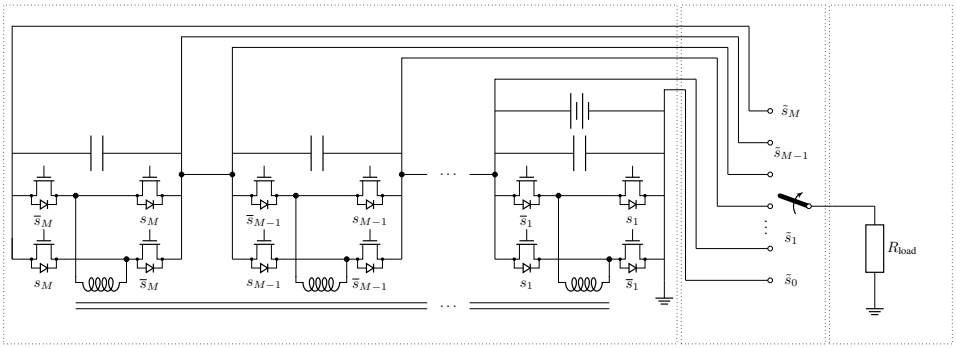

Figure 2: Circuit diagram of the proposed converter. The components from left to right are the DC-autotransformer, the tap selector, the PWM module, and a resistive load as assumed to be connected in this paper. The converter is fed by a DC-source which is connected to the DC-autotransformer.

Equation (4) is a linear equation for $\frac{\mathrm{d}i_m}{\mathrm{d}t}$. Using $i_m = \sum_{i=1}^{M} i_i$ we obtain the following expression:

$$\begin{aligned}\frac{\mathrm{d}i_m}{\mathrm{d}t} &= \frac{1}{L_s}\sum_{i=1}^{M} V_i \cdot s_i(t) - \frac{R}{L_s}\sum_{i=1}^{M} i_i + \\ &\quad -M\frac{R_m}{L_s}\cdot\sum_{i=1}^{M} i_i - M\frac{L_m}{L_s}\frac{\mathrm{d}i_m}{\mathrm{d}t} \\ &= \frac{\sum_{i=1}^{M} V_i \cdot s_i(t)}{L_s + ML_m} - \frac{R + MR_m}{L_s + ML_m}\sum_{i=1}^{M} i_i \end{aligned} \quad (5)$$

Applying (5) to (2) yields the system ordinary differential equation for the current:

$$\begin{aligned}\frac{\mathrm{d}}{\mathrm{d}t}i_k &= \frac{1}{L_s}V_k \cdot s_k(t) - \frac{R}{L_s}i_k - \frac{R_m}{L_s}\sum_{i=1}^{M} i_i + \\ &\quad -\frac{L_m}{L_s}\left(\frac{\sum_{i=1}^{M} V_i \cdot s_i(t)}{L_s + ML_m} - \frac{R + MR_m}{L_s + ML_m}\sum_{i=1}^{M} i_i\right) \\ &= \frac{1}{L_s}V_k \cdot s_k(t) - \frac{R}{L_s}i_k - \frac{L_m\sum_{i=1}^{M} V_i \cdot s_i(t)}{L_s(L_s + ML_m)} + \\ &\quad + \frac{L_m R - L_s R_m}{L_s(L_s + ML_m)}\sum_{i=1}^{M} i_i. \end{aligned} \quad (6)$$

The dynamics of the voltage V_k at the DC-link is given by the DC-link current which is equal to the negative AC-current multiplied by the switching state:

$$\frac{\mathrm{d}}{\mathrm{d}t}V_k = -\frac{1}{C_{\text{dc}}}s_k(t)i_k. \quad (7)$$

With the differential equations (6) and (7) we can assemble a state space model $\mathbf{x} \in \mathbb{R}^{2M}$:

$$\mathbf{x} = \begin{bmatrix} i_1 & V_1 & i_2 & V_2 & \dots & i_M & V_M \end{bmatrix}^T. \quad (8)$$

This allows formulating a system model

$$\dot{\mathbf{x}} = \mathbf{A}_{\text{DC}}(s_1, .., s_M)\mathbf{x} \quad (9)$$

where $\mathbf{A}_{\text{DC}}(s_1, .., s_M) \in \mathbb{R}^{2M\times 2M}$ is the system matrix which is depending on the switching states s_i. Defining

$$L_{\text{sys}_1} = \frac{L_s + (M-1)L_m}{L_s^2 + L_m L_s M}, \quad (10)$$

$$L_{\text{sys}_2} = \frac{L_m}{L_s^2 + L_m L_s M}, \quad (11)$$

$$R_{\text{sys}_1} = \frac{2(1-M)RL_m - R_m L_s - 2RL_s}{L_s^2 + L_m L_s M} \quad (12)$$

$$R_{\text{sys}_2} = \frac{2RL_m - R_m L_s}{L_s^2 + L_m L_s M} \quad (13)$$

it is given by

$$\mathbf{A}_{\text{DC}} = \begin{bmatrix} R_{\text{sys}_1} & s_1 L_{\text{sys}_1} & \dots & -s_M L_{\text{sys}_2} \\ -s_1\frac{1}{C_{\text{dc}}} & 0 & \dots & 0 \\ \vdots & \vdots & \ddots & \vdots \\ R_{\text{sys}_2} & -s_1 L_{\text{sys}_2} & \dots & s_M L_{\text{sys}_1} \\ 0 & 0 & \dots & 0 \end{bmatrix}. \quad (14)$$

If a resistive load R_l is connected to one of the ports and the ground (compare Figure 2), the system model can be extended as follows:

$$\dot{\mathbf{x}} = (\mathbf{A}_{\text{DC}} + \mathbf{A}_{\text{L}})\,\mathbf{x} \quad (15)$$

where $\mathbf{A}_{\text{L}} \in \mathbb{R}^{2M\times 2M}$ represents the influence of the load. It is given by

$$\mathbf{A}_{\text{L}} = \begin{bmatrix} \mathbf{A_1} & \mathbf{A_2} & \dots & \mathbf{A_M} \\ \mathbf{A_2} & \mathbf{A_2} & \dots & \mathbf{A_M} \\ \vdots & \vdots & \ddots & \vdots \\ \mathbf{A}_M & \mathbf{A}_M & \dots & \mathbf{A_M} \end{bmatrix}, \quad (16)$$

$$\mathbf{A_i} = \begin{bmatrix} 0 & 0 \\ 0 & s\cdot\sum_{j=i}^{M}\tilde{s}_j\frac{1}{C_{\text{dc}}R_{\text{Load}}} \end{bmatrix}. \quad (17)$$

where $\tilde{s}_j = 1$ if module j is connected to the load and $\tilde{s}_j = 0$ otherwise.

IV. Simulation Results

To verify the proposed system, a simulation model has been constructed in Simscape. The model has $M = 4$ modules an input voltage of 100 V connected in series to the first module.

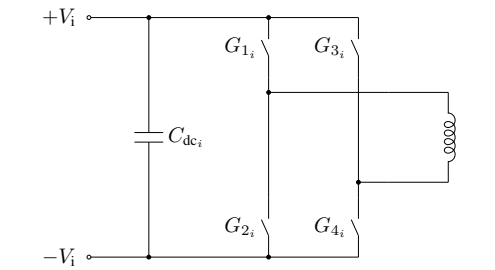

(a) Active Bridge Topology

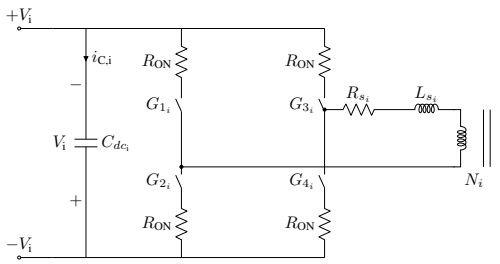

(b) Model used in this paper

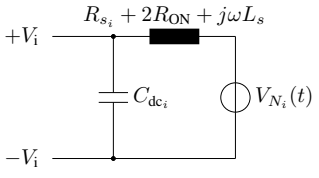

(c) Equivalent circuit using source and internal resistance

Figure 3: Circuit diagram of an active bridge. The first subfigure shows the basic topology with the DC-voltage. The switches G_{1_i} and G_{4_i} are switched together, alternating with G_{2_i} and G_{3_i}. In this way, an AC-voltage is generated at the winding. The second inset shows the equivalent used in this paper, based on the assumptions stated in section III. The switches are modelled as an ON-state resistance. The transformer is modeled as a winding resistance and a stray inductance. Not shown is the magnetization inductance and resistance which occurs only in the first winding. The third inset shows a simplified equivalent circuit using a source and internal resistance summarized from the equivalent circuit in (b). For the given system, the source as well as the resistor are time-varying.

In this case, the first module capacitance does not contribute to the dynamics and some entries of the system matrix have to be modified. Furthermore, a magnetization inductance of $L_m = 20\mu$H, a DC-link capacitance of $V_{\mathrm{dc}} = 20\mu$C, a load of $R_{\mathrm{Load}} = 10\Omega$, a stray inductance of $L_s = 0.1$ nH and a conduction resistance of 0.025Ω are used. The operating frequency of the multiactive bridge was set to 100 kHz and all bridges were switched synchronously with a duty-cycle of $D = 0.5$. The Simscape model was then compared to a prediction based on the differential equation derived in the paper. During the simulation, all switches are synchronously,

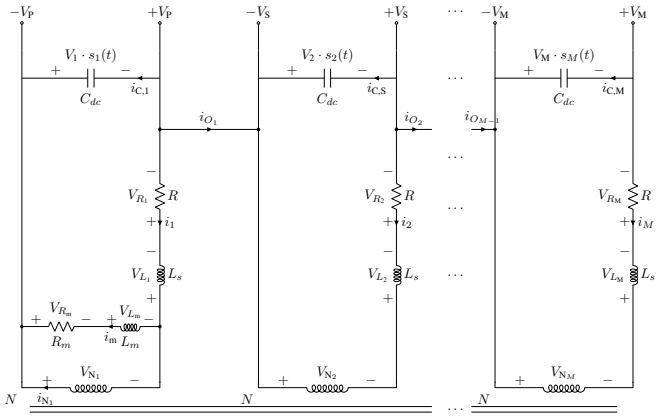

Figure 4: Equivalent Circuit diagram of the M-active bridge converter in DC-autotransformer configuration. The circuit is shown from the transformer point of view. The topology change which is induced by the switching is represented by the signal $s_i(t)$ for $i = 1, ..., M$.

i.e. $s_1(t) = s_2(t) = ... = s_M(t) =: s(t)$.

A. Results for the Loadless Case

In the loadless case, the only input to the system is the switching state $s(t)$. The results are shown in Fig. 6a for the DC-Voltages and Fig. 6b for the AC-currents. In both, the system states oscillate with the frequency of $s(t)$, around the supply voltage V_{dc} in case of the DC-voltages and around 0 A in case of the AC-currents. The frequency of the oscillations stays constant while they lose in amplitude. This can be explained by convergence to a balanced voltage state. The change in behaviour of the system with respect to the frequency of $s(t)$ is shown in Fig. 5. It can be seen that changing the frequency of $s(t)$ has no influence on the phase shift of the AC-currents as shown in Fig. 5b. Increasing the frequency does however yield a lower amplitude of the oscillations which is shown in Fig. 5a.

B. Results for the System under Load

Figure 6b and 6a show the results of all system variables during load voltage change. A step response is given to the load voltage which is implemented as a change in the module that is connected to the load from $\tilde{s}_1$ to $\tilde{s}_2$ at $t = 10$ μs which is after one period of the multi-active bridge. While V_1 stays constant since it is connected to the voltage source, all other voltages experience a slight drop. The sharpest drop is shown in the second module since the load now discharges the DC-link capacitor of this module. The other modules try to balance the multi-active bridge and discharge their DC-links as well using their winding currents. This can be seen in the simulation as well as the prediction in Fig. 6b. A similar observation can be made for the current: during the first period, a slight oscillation is visible that is increased with the load voltage. In addition to that, the AC-current of the module that has the load connected now oscillates with a 180° phase shift compared to the other modules. This observation can again be explained

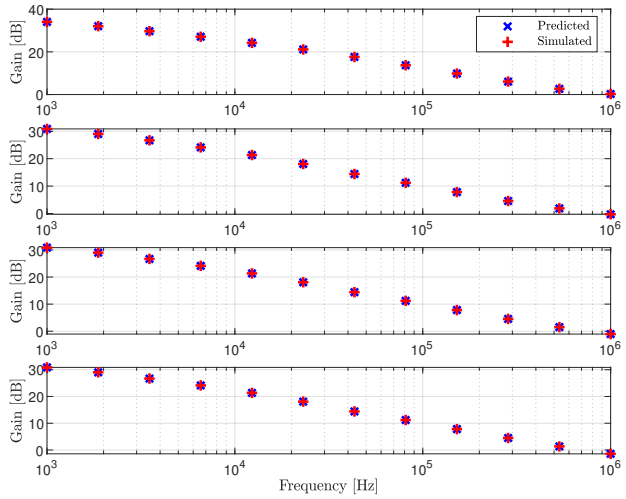

(a) Steady-State Simulation Results of the gains of the AC-Currents

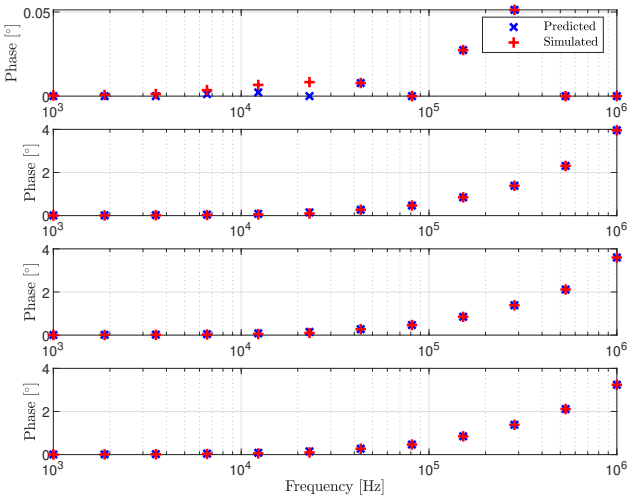

(b) Steady-State Simulation Results of the shifts of the AC-Currents

Figure 5: Simulation Results of all system variables for different frequencies of $s(t)$. The gain is here defined as the change of amplitude of the current signal in comparison with the a signal of amplitude 1. The amplitude is defined as the average distance between the maximum and minimum of the signal. The phase is defined as the delay of the given quantity in comparison to the switching signal $s(t)$.

by taking the balancing of the system into account. Modules 3 and 4 create currents that discharge their DC-link capacitors and module 1 stays constant only due to the voltage source that is connected to it. The phase shift in the current of the second module implies that the discharging current of the other modules is used by the second module to charge its DC-link capacitor and compensate for the effects of the load. Moreover, at $t = 15\ \mu$s, the charging current is large enough to reduce the voltage drop in the second module, and the decrease in DC-link voltage slows down. A detailed look at the load voltage change in Fig. 7a for the DC-voltages and Fig. 7b for the AC-currents shows the small error of the model compared to the simulation. The curve of the prediction differs only slightly from the simulation for the voltages while the currents have a small deviation during the switching process.

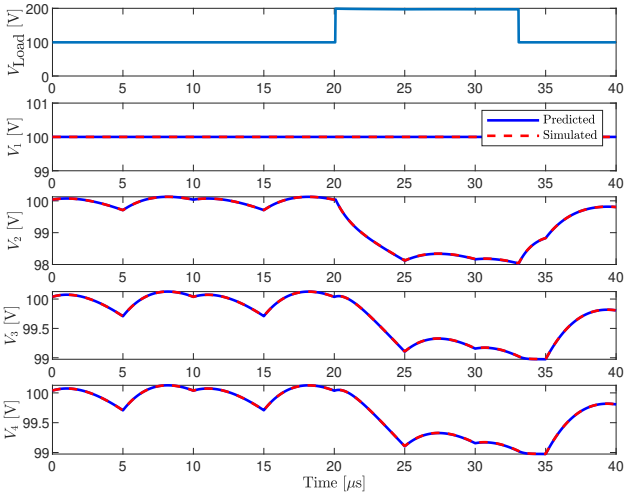

(a) Simulation Results DC- Voltages

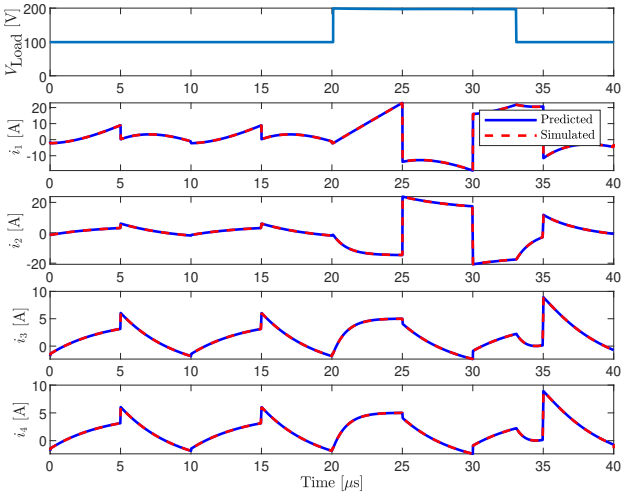

(b) Simulation Results AC- Currents

Figure 6: Simulation Results of all state-space variables. A step in load voltage from 100 V to 200 V is given to the system 20μs. At 28μs the load voltage is set back to 100 V. The first inset of both subfigures shows the load voltage, i.e. which modules are connected to the load. The remaining plots show the response of all system variables of the system for both, the predicted and simulated system for comparison.

V. Conclusion

We introduced a modeling approach to a novel multi-winding transformer-based converter. The transformer is modeled as an N-port network with magnetization and stray inductance. The proposed model, while being simple and requiring few parameters, is still accurate enough to give detailed insight into the behavior of each submodule. Furthermore, it can be used to describe and quantify advanced phenomena of the topology such as transformer currents, the

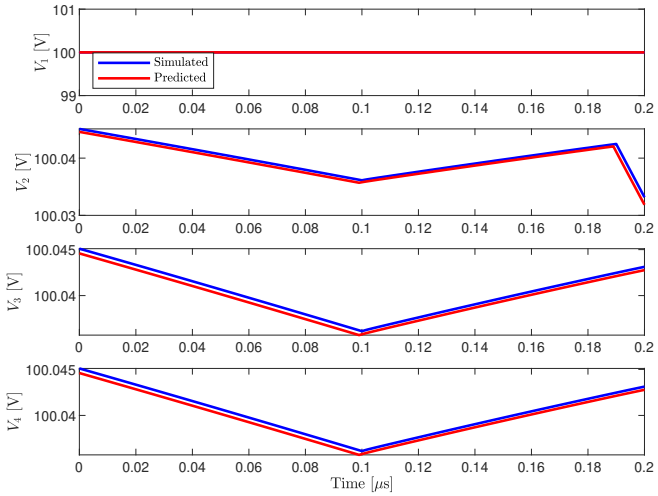

(a) Module DC-voltages

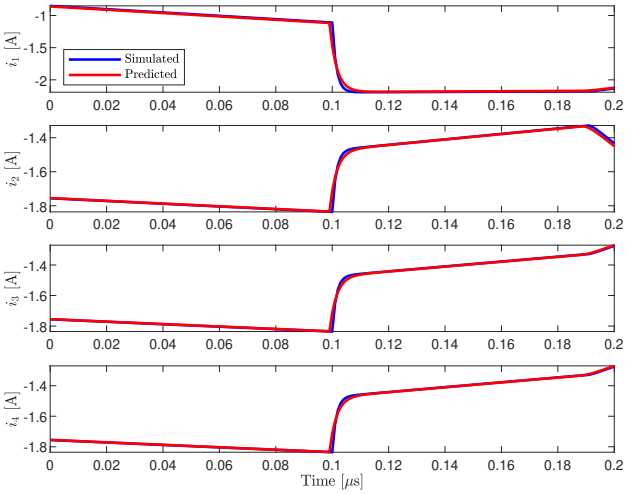

(b) Module AC- Currents

Figure 7: Details of the simulation result at the load voltage jump from 100V to 200V. The jump occurs at the time 0.1 μs. The simulated curves are shown in blue while the predicted ones are shown in red. The top subfigure shows the DC-voltages while the bottom subfigure shows the AC-current in each of the modules.

switching state in the active bridges, and submodule balancing. Simulation results validate the accuracy of the system model under various conditions. In case of experimental verification, the assumptions mentioned in section III. need to be tested, especially the negligible cross-coupling and parasitic inter-winding capacitances.

REFERENCES

[1] C. Zhao, S. D. Round, and J. W. Kolar, "An isolated three-port bidirectional dc-dc converter with decoupled power flow management," *IEEE Transactions on Power Electronics*, vol. 23, no. 5, pp. 2443–2453, 2008.

[2] R. W. A. A. De Doncker, D. M. Divan, and M. H. Kheraluwala, "A three-phase soft-switched high-power-density dc/dc converter for high-power applications," *IEEE Transactions on Industry Applications*, vol. 27, no. 1, pp. 63–73, 1991.

[3] P. Wang and M. Chen, "Towards power fpga: Architecture, modeling and control of multiport power converters," in *2018 IEEE 19th Workshop on Control and Modeling for Power Electronics (COMPEL)*, 2018, pp. 1–8.

[4] Y. Chen, P. Wang, H. Li, and M. Chen, "Power flow control in multi-active-bridge converters: Theories and applications," in *2019 IEEE Applied Power Electronics Conference and Exposition (APEC)*, 2019, pp. 1500–1507.

[5] M. Liu, Y. Chen, Y. Elasser, and M. Chen, "Dual frequency hierarchical modular multilayer battery balancer architecture," *IEEE Transactions on Power Electronics*, vol. 36, no. 3, pp. 3099–3110, 2021.

[6] J. Wood, E. Shelton, K. Rathbone, M. Baghdadi, T. Regan, and P. Palmer, "Adiabatic dc-ac power converter with 99% efficiency," in *PCIM Europe 2016: Proceedings of International Exhibition and Conference for Power Electronics, Intelligent Motion, Renewable Energy and Energy Management*. IEEE, 2016, pp. 1–8.

[7] A. Schellmanns, J.-P. Keradec, J.-L. Schanen, and K. Berrouche, "Representing electrical behaviour of transformers by lumped element circuits: a global physical approach," in *Conference Record of the 1999 IEEE Industry Applications Conference. Thirty-Forth IAS Annual Meeting (Cat. No.99CH36370)*, vol. 3, 1999, pp. 2100–2107 vol.3.

[8] R. Erickson and D. Maksimovic, "A multiple-winding magnetics model having directly measurable parameters," in *PESC 98 Record. 29th Annual IEEE Power Electronics Specialists Conference (Cat. No.98CH36196)*, vol. 2, 1998, pp. 1472–1478 vol.2.

[9] Z. De Gréve, O. Deblecker, J. Lobry, and J.-P. Kéradec, "High-frequency multi-winding magnetic components: From numerical simulation to equivalent circuits with frequency-independent rl parameters," *IEEE Transactions on Magnetics*, vol. 50, no. 2, pp. 141–144, 2014.

[10] L. I. Sakhno and N. A. Smorygin, "Numerical calculation of the impedance of the resistance spot welding machines transformer," in *2018 IEEE Conference of Russian Young Researchers in Electrical and Electronic Engineering (EIConRus)*, 2018, pp. 227–230.

[11] C. Jäschke and P. Schegner, "Analytic computation of the magnetizing inductance of current instrument transformers under consideration of eddy currents," *IEEE Transactions on Magnetics*, vol. 51, no. 11, pp. 1–4, 2015.

[12] W. Tan, X. Margueron, L. Taylor, and N. Idir, "Leakage inductance analytical calculation for planar components with leakage layers," *IEEE Transactions on Power Electronics*, vol. 31, no. 6, pp. 4462–4473, 2016.

[13] Z. Zheng, Z. Gao, C. Gu, L. Xu, K. Wang, and Y. Li, "Stability and voltage balance control of a modular converter with multiwinding high-frequency transformer," *IEEE Transactions on Power Electronics*, vol. 29, no. 8, pp. 4183–4194, 2014.

[14] C. Gu, Z. Zheng, L. Xu, K. Wang, and Y. Li, "Modeling and control of a multiport power electronic transformer (pet) for electric traction applications," *IEEE Transactions on Power Electronics*, vol. 31, no. 2, pp. 915–927, 2016.

[15] S. Okutani, P. Huang, and Y. Kado, "Generalized average model of triple active bridge converter," in *2019 IEEE Energy Conversion Congress and Exposition (ECCE)*, 2019, pp. 5554–5560.

[16] S. Falcones, R. Ayyanar, and X. Mao, "A dc–dc multiport-converter-based solid-state transformer integrating distributed generation and storage," *IEEE Transactions on Power Electronics*, vol. 28, no. 5, pp. 2192–2203, 2013.

[17] L. Ortega, P. Zumel, C. Fernández, J. López-López, A. Lázaro, and A. Barrado, "Power distribution algorithm and steady-state operation analysis of a modular multiactive bridge converter," *IEEE Transactions on Transportation Electrification*, vol. 6, no. 3, pp. 1035–1050, 2020.

[18] M. A. Rahman, M. R. Islam, K. M. Muttaqi, and D. Sutanto, "Modeling and control of sic-based high-frequency magnetic linked converter for next generation solid state transformers," *IEEE Transactions on Energy Conversion*, vol. 35, no. 1, pp. 549–559, 2020.

[19] S.-P. Hsu, "Problems in analysis and design of switching regulators : I. pole placement technique for dc-to-dc switching regulators. ii. transformer modelling. iii. cross-regulation of the two-output cuk converter," Ph.D. dissertation, California Institute of Technology, 1980.